Journal of Molecular Liquids 340 (2021) 117272

Contents lists available at ScienceDirect

Journal of Molecular Liquids

journal homepage: www.elsevier.com/locate/molliq

Solubility of xenon in liquid *n*-alkanes and cycloalkanes by computer simulation. Towards the perfect anaesthetic

Luís F.G. Martins [a,b,*], Alfredo J. Palace Carvalho [a], Pedro Morgado [b], Eduardo J.M. Filipe [b]

[a] LAQV-REQUIMTE - Évora, Institute for Research and Advanced Studies, School of Science and Technology, University of Évora, Rua Romão Ramalho 59, 7000-671 Évora, Portugal
[b] Centro de Química Estrutural, Instituto Superior Técnico, Universidade de Lisboa, Av. Rovisco Pais, 1049-001 Lisboa, Portugal

ARTICLE INFO

Article history:
Received 12 June 2021
Revised 2 August 2021
Accepted 10 August 2021
Available online 18 August 2021

Keywords:
Xenon
N-alkanes
Cycloalkanes
Henry's constants
Monte Carlo simulations
Interaction energy

ABSTRACT

The solubility (Henry's constant) of xenon in a series of *n*-alkanes (*n*-heptane, *n*-octane, *n*-nonane, *n*-dodecane and *n*-hexadecane) and in two cycloalkanes (cyclopentane and cyclohexane) has been obtained by Monte Carlo computer simulations as a function of temperature, at a reference pressure of 100 kPa and compared with experimental results from literature. The *n*-alkanes and cycloalkanes were modelled with the united atom TraPPE force field, using optimized non-bonded parameters in a transferable fashion for each solvent family. Standard enthalpies of solvation were calculated from the temperature dependence of the Henry's constants. Solute-solvent interaction energies were also estimated for all systems by Molecular Dynamics. The agreement between the simulated Henry's constants and experimental data from the literature is excellent in all cases. For all systems involving *n*-alkanes, the temperature dependence of the standard enthalpies of solvation displays a maximum at very similar reduced temperatures, $0.51 < T_R < 0.55$. These results confirm the behaviour previously observed experimentally for *n*-pentane and *n*-hexane. Furthermore, the simulation results provide a large coherent set of data that allows extending the analysis to a large number of longer *n*-alkanes, including those for which no experimental data is available.

Structural details of the solutions were also studied calculating the radial distribution functions xenon/CH_n for all the systems at similar thermodynamic states. The results confirm the enrichment of methyl groups within xenon's first coordination sphere relatively to methylene groups. The effect is more pronounced the longer the *n*-alkane chain.

1. Introduction

Gaseous xenon is a well-known inhalation anaesthetic. With no side effects, rapid emergence, a low minimum alveolar concentration (MAC) of 0.6–0.7 atm as well as neuroprotectant and cardioprotectant properties, xenon has been considered an almost perfect anaesthetic [1]. Although the molecular mechanism of anaesthesia is far from being fully understood, it has been shown that xenon can act on NMDA membrane receptors [2], exerting effects on nicotinic acetylcholine receptors [3] and certain potassium channels [4]. However, most of the studies on xenon anaesthetic mechanisms have been directed to its action on the nerve cell membrane. Xenon tends to increase the area per lipid, changing the thickness and the local and global lipid order in model membranes [5,6] and is able to change the phase distribution of membrane lipid raft mixtures to favor the disordered phase [7]. It is also known that xenon, in contact with model membranes, tends to be localized in the middle of the bilayer, but also just below the lipid head group. This latter location is very important given the changes it produces in membrane structure and dynamics [8]. The structural simplicity of xenon in comparison with other more complex anaesthetic families seems to exclude specific interactions as the basis of its anaesthetic action. Thus, studying the structure and interactions of xenon within lipid bilayers, which are mostly formed by alkylic chains, can be an important contribution to deepen the knowledge of the anaesthetic action of xenon.

The study of molecular/segmental interactions and liquid structure (repulsive forces) of simple molecules and their mixtures is a topic of high scientific interest [9,10], since it is very often the ultimate result of the decomposition of complex problems, where the theoretical explanations from first principles are more easily applied and understood. Important and up-to-date scientific phenomena observed in more complex systems, such as the formation and behaviour of different domains in ionic liquids [11] or the

* Corresponding author.
E-mail address: lfgm@uevora.pt (L.F.G. Martins).

https://doi.org/10.1016/j.molliq.2021.117272
0167-7322/

self-organization in partially fluorinated organic compounds [12,13] often require explanations that can be based on studies done using simple molecules, whose results are more prone to separate effects and distinguish trends.

Noble gases and alkanes have long been used as model substances to study the effect of size, shape and flexibility on the thermodynamic properties of fluid mixtures [14–18]. The absence of molecular structure of the noble gases (in other words, their isotropic intermolecular potential) allows their use as reference particles, comparing the properties of their binary mixtures with components of different shapes and polarities. In particular, the large polarizability of xenon is known to amplify binary interactions, which makes this noble gas particularly useful as a test particle. On the other hand, the *n*-alkanes larger than *n*-butane form a chemical family whose properties change in a very regular way. The exceptional behaviour of the first three members of the *n*-alkane family, as well as a number of model branched alkanes and cycloalkanes, allows instructive discussions on the effect of shape, segmental interaction, rigidity and packing. Solubility data at infinite dilution and derived thermodynamic quantities are important properties to study solute–solvent interaction in the absence of solute–solute contacts, probing the solvent organization around the solute molecule. On the other hand, computer simulations have become essential tools to establish the desired link between macroscopic properties and molecular level phenomena [19].

Pollack *et al.* measured the solubility of xenon in a series of *n*-alkanes, (C_5 - C_{16}) [20], cycloalkanes (C_5, C_6 and C_8) and in a variety of organic solvents [21]. However, measurements were performed within a relatively narrow temperature range. Thus, the standard enthalpies and entropies of solvation, estimated from the experimental results, were assumed to be constant within the studied temperature range. The average standard enthalpy of solvation for xenon in *n*-alkanes was found to increase (becomes less negative) with the increasing chain length of the solvent and to be less negative for cycloalkanes than for *n*-alkanes.

In a previous work, we reported measurements of the solubility of xenon in *n*-pentane and *n*-hexane [22,23]. In our case, measurements were performed in a wider temperature range and using a more accurate temperature control, which enabled estimating the enthalpy of solvation (ΔH_2^0) as a function of temperature. It was found that for xenon in *n*-pentane and *n*-hexane ΔH_2^0 first increases with temperature, at lower temperatures, and then decreases, exhibiting a maximum at approximately the same reduced temperature for both systems, 0.53–0.54. Interestingly, this is very close to the reduced temperature at which the excess enthalpy for equimolar mixtures of *n*-alkanes changes from positive to negative. This result was seen as an additional example of the similarity between (xenon + *n*-alkane) and (*n*-alkane + *n*-alkane) interactions [17,24]. Monte Carlo simulations, using the TraPPE united atom model [25] and SAFT-VR calculations [26] produced Henry's constants in close agreement with experiment.

In a more recent work, we combined ^{129}Xe NMR measurements as a function of temperature, with molecular dynamics simulations, to study solutions of xenon in linear, cyclic and branched alkanes [27]. Several important conclusions could be drawn from this study. Firstly, it was shown that xenon interacts more intensely with methyl than with methylene groups, due to the larger number of hydrogen atoms in the former. It was also found that the CH_2 units of cycloalkanes seem to be less interactive towards xenon than those of *n*-alkanes. It was demonstrated that this is a subtle consequence of the shape of cyclic molecules, which allows different degrees of access of the xenon atom to the different CH_2 units forming a cycloalkane molecule. Finally, it was also shown that the relative distribution of methylene and methyl groups around xenon does not match their stoichiometric proportion in the solvent molecule. Instead, a relative enrichment of CH_3 groups is observed in the xenon's first coordination sphere, increasing with the chain length of the solvent. Perhaps more importantly, this work highlighted the potential of ^{129}Xe NMR spectroscopy to probe the structure and interactions of fluids, and the importance of conducting those studies at similar thermodynamics conditions. The same strategy has been recently extended to study *n*-perfluoroalkanes [28], *n*-perfluoroalkylalkanes [29], and ionic liquids [30].

Mixtures involving xenon and cycloalkanes have also been studied in our research group [16,31–32]. Solutions of xenon in cyclopentane in a wider temperature range were recently reported [33]. Comparing with (xenon + *n*-pentane), both enthalpy and entropy of solvation show opposite temperature dependences. For (xenon + *n*-pentane) both enthalpy and entropy of solvation decrease with increasing temperature above T_r = 0.54 (being T_r the system temperature divided by the critical temperature of the solvent). For (xenon + cyclopentane) these two properties increase monotonously with temperature, showing that the heat capacities of solvation display opposite signals for aliphatic and cyclic solvents. This behavior was explained recurring to the "condensation" effect proposed in the 1970s by Patterson [34–36], which suggests that linear alkanes tend to "condense" at the surface of highly branched, rigid and sterically hindered molecules, restricting molecular motion, thus leading to negative contributions to excess enthalpy and entropy and positive contributions to excess heat capacity. Molecules with plate-like anisotropic structures like cyclopentane, cyclopropane and cyclobutane, would favor the condensation of *n*-alkanes and xenon on their surface [16,31].

In the present work, we have extended the computer simulation studies of xenon in *n*-alkanes to longer members of the series (*n*-heptane, *n*-octane, *n*-nonane, *n*-dodecane and *n*-hexadecane). Henry's constants were obtained for all the systems by Monte Carlo simulations at 100 kPa and as a function of temperature, using the united atom TraPPE force field. The simulation results are in excellent agreement with experimental data from the literature demonstrating the ability of the model used to describe such systems. Moreover, the results confirm the behaviour previously observed experimentally for *n*-pentane and *n*-hexane: standard enthalpies of solvation calculated from the temperature dependence of the Henry's constants display a maximum at very similar reduced temperatures, $0.51 < T_r < 0.55$. Thus, the simulation results provide a large coherent set of data for the longer *n*-alkanes, for which experimental data was lacking or existed only within a very narrow temperature range.

Solutions of xenon in two cycloalkanes (cyclopentane and cyclohexane) were also simulated and solute–solvent interaction energies were obtained for all systems by Molecular Dynamics. The structure of xenon's coordination sphere is also discussed, based on the analysis of the radial distribution functions between the solute and each molecular group of the solvent molecules.

2. Simulation details

The Henry's constants for xenon in liquid *n*-heptane, *n*-octane, *n*-nonane, *n*-dodecane, *n*-hexadecane, cyclopentane and cyclohexane as a function of temperature at 100 kPa were obtained by computer simulation using Widom's test-particle insertion algorithm [37]. The method uses Monte Carlo simulations to compute the excess chemical potential ($\mu_2^{exc.,\infty}$) of the solute 2 in the solvent 1 at infinite dilution, which in turn allows the calculation of Henrýs constant by the well-known relation:

$$H_{2,1}(T,p) = \lim_{x_2 \to 0} \left[RT\rho_1 \exp\left(\mu_2^{exc.,\infty}/RT\right)\right] \quad (1)$$

where $\mu_2^{exc,\infty}$ is the excess chemical potential (the difference between the chemical potential of solute 2 in solvent 1 at infinite dilution and the chemical potential of pure species 2 at ideal gas state), T is temperature, p is pressure, ρ_1 is the density of the pure solvent and R is the ideal gas constant.

The excess chemical potential at infinite dilution is calculated by the equation:

$$\mu_2^{exc.,\infty} = -RT \ln \left[\frac{\langle V exp(-u_{TP}/kT) \rangle_{NpT}}{\langle V \rangle_{NpT}} \right] \quad (2)$$

where u_{TP} is the interaction energy of the test particle with a configuration of solvent molecules, V is the volume of solvent in a given configuration, R is the ideal gas constant, T is temperature and $\langle \ldots \rangle_{NpT}$ denotes an isothermal-isobaric ensemble average.

For the Henry's constants calculations, the computer simulations were performed using the MCCCS Towhee Monte Carlo molecular simulation package, version 6.2.2 [38]. The calculation of radial distribution functions (*rdf*) and the solute–solvent interaction energies were done from molecular dynamics simulations performed using the GROMACS package (version 4.5.7) [39,40]. The force field used to describe all the *n*-alkanes was based on TraPPE-UA [41] whose main characteristics are fixed bond lengths, harmonic style angle bending terms and quadratic torsion terms for the intramolecular interactions, whereas the intermolecular terms are modelled by Lennard-Jones potentials centred on the carbon atoms. This is a united atom force field, which means that CH_n groups are modelled as single pseudo-atoms. In this work we used the same parameters as Bonifácio *et al* [23], which had been obtained by Laginhas *et al* [42], using the Martin *et al* [41] (for CH_3 and CH_2 sites on *n*-alkanes) and Bohn *et al* [43] (for xenon) parameters as starting points. In the case of cycloalkanes, Lennard-Jones parameters for the CH_2 unit were obtained in this work by fitting to the experimental densities of cyclopentane (from reference [44]) as a function of temperature (average deviation: 0.10 %). These parameters reproduce the experimental density of cyclohexane (also from reference [44]), at 1 bar and between 280 K and 350 K, with an average deviation of 4%. It must be pointed out that, with the original CH_2 parameters by Martin *et al.,* the simulated densities of cyclopentane at 1 bar deviated between 7 and 13 % from experiment (in the 180–310 K range), and for cyclohexane deviated between 2 and 13 % (from 280 to 350 K) [42]. For the *n*-alkanes (from *n*-heptane to *n*-hexadecane), the refined parameters reproduce the experimental liquid densities at 1 bar with average deviations from 0.24 to 0.62 %, with the density of *n*-hexadecane being particularly well predicted. All of the parameters used for interactions between like sites are shown in table 1. The unlike parameters were obtained using the Lorentz-Berthelot combination rules, which means that no experimental results for mixtures were needed to predict Henry's constants.

For the determination of Henry's constants, the calculations were carried out in the *NpT* ensemble with a single box having side lengths of approximately 35–40 Å and containing between 250 and 400 solvent molecules. In each simulation, a preliminary solvent equilibration run of between 50,000 and 150,000 steps (each step consisting of a number of moves equal to the number of molecules in the system) was done, followed by a production run consisting of another 200,000 steps, which were divided into 20 blocks in order to calculate standard deviations. 1000 insertions of a solute

Table 1
Non-bonded parameters for each interaction site used in this work for computer simulation calculations.

	(ε/k_B) /K	σ /Å
CH_3	100.75	3.787
CH_2	47.2	4.03
CH_2 (cyclic)	56	3.85
Xe	226.3	3.948

Table 2
Henrýs constants and their statistical uncertainties for xenon in *n*-heptane, *n*-octane, *n*-nonane, *n*-dodecane and *n*-hexadecane at 100 kPa as a function of temperature, obtained from the Monte Carlo simulations.

	Xenon in *n*-heptane		Xenon in *n*-octane		Xenon in *n*-nonane	
T/K	$H_{2,1}$/MPa	$\delta H_{2,1}$/MPa	$H_{2,1}$/MPa	$\delta H_{2,1}$/MPa	$H_{2,1}$/MPa	$\delta H_{2,1}$/MPa
275	2.82	0.16	2.80	0.20	2.65	0.22
280	3.08	0.13	2.97	0.11	2.94	0.27
285	3.31	0.15	3.22	0.20	3.15	0.23
290	3.56	0.13	3.47	0.17	3.37	0.19
295	3.75	0.14	3.82	0.20	3.57	0.18
300	3.97	0.17	3.95	0.17	3.88	0.22
305	4.19	0.17	4.18	0.13	4.13	0.24
310	4.57	0.16	4.46	0.22	4.39	0.21
315	4.83	0.13	4.67	0.14	4.70	0.24
320	5.12	0.17	5.01	0.19	4.89	0.18
325	5.34	0.14	5.29	0.19	5.26	0.23
330	5.67	0.18	5.61	0.21		
	Xenon in *n*-dodecane		Xenon in *n*-hexadecane			
T/K	$H_{2,1}$/MPa	$\delta H_{2,1}$/MPa	$H_{2,1}$/MPa	$\delta H_{2,1}$/MPa		
280	2.70	0.29				
285	2.92	0.21				
290	3.11	0.18				
295	3.35	0.29	3.02	0.30		
300	3.66	0.31	3.35	0.42		
305	3.92	0.25	3.49	0.45		
310	4.05	0.30	3.73	0.30		
315	4.30	0.28	3.78	0.42		
320	4.62	0.16	4.14	0.41		
325	4.76	0.23	4.29	0.40		
330	5.04	0.18	4.62	0.34		
335	5.38	0.26	4.75	0.23		
340	5.60	0.27	5.15	0.26		
345	5.83	0.30	5.19	0.28		
350	6.09	0.36	5.32	0.38		
355	6.32	0.21	5.64	0.26		
360	6.64	0.33	6.04	0.33		
365	6.90	0.25	6.24	0.38		
370	7.21	0.25	6.24	0.33		
375			6.51	0.30		
380			6.92	0.35		

Table 3
Henrýs constants and their statistical uncertainties for xenon in cyclopentane and cyclohexane at 100 kPa as a function of temperature, obtained from the Monte Carlo simulations.

	Xenon in cyclopentane		Xenon in cyclohexane	
T/K	$H_{2,1}$/MPa	$\delta H_{2,1}$/MPa	$H_{2,1}$/MPa	$\delta H_{2,1}$/MPa
250	2.18	0.27		
255	2.44	0.27		
260	2.64	0.24		
265	2.77	0.29		
270	3.17	0.25		
275	3.48	0.28		
280	3.68	0.28	4.00	0.53
285	3.89	0.28	4.49	0.46
290	4.28	0.28	4.81	0.48
295	4.51	0.35	5.11	0.28
300	4.85	0.34	5.34	0.46
305	5.21	0.40	5.65	0.32
310	5.53	0.26	6.08	0.45
315	5.83	0.32	6.56	0.44
320			6.75	0.29
325			7.15	0.33
330			7.64	0.35
335			7.86	0.48
340			8.34	0.28
345			8.66	0.52
350			9.25	0.45

test particle were done for each MC production step (for a total of 2×10^8 insertions per run). The Monte Carlo moves consisted of simulation box volume changes, coupled-decoupled configurational-bias re-growths, translations of the centre of mass, rotations about the centre of mass and configurational-bias molecule reinsertions in the simulation box. Henry's constant calculations were done as a function of temperature, in 5 K intervals, from 275 K to 330 K for xenon in *n*-heptane and *n*-octane, from 275 K to 325 K for *n*-nonane, from 280 to 370 K for *n*-dodecane, from 295 K to 380 K for *n*-hexadecane, from 250 K to 315 K for cyclopentane and from 280 K to 350 K for cyclohexane. The system pressure was fixed at 100 kPa.

For the determination of radial distribution functions, molecular dynamics simulations were performed, in boxes containing 500 to 800 solvent molecules and a number of xenon molecules corresponding to the respective solubility in each solvent. Solute-solvent interaction energies were also determined by molecular dynamics simulations, using 250 to 400 solvent molecules and one xenon molecule. For both cases, the initial box volumes were chosen according to the experimental densities of the systems. After an energy minimization run for system relaxation, the boxes were equilibrated during 2 to 16 ns, followed by 8 to 16 ns production runs, in all cases with a time-step of 1 fs. A cut-off distance of 12 Å was used for the dispersive interactions, with

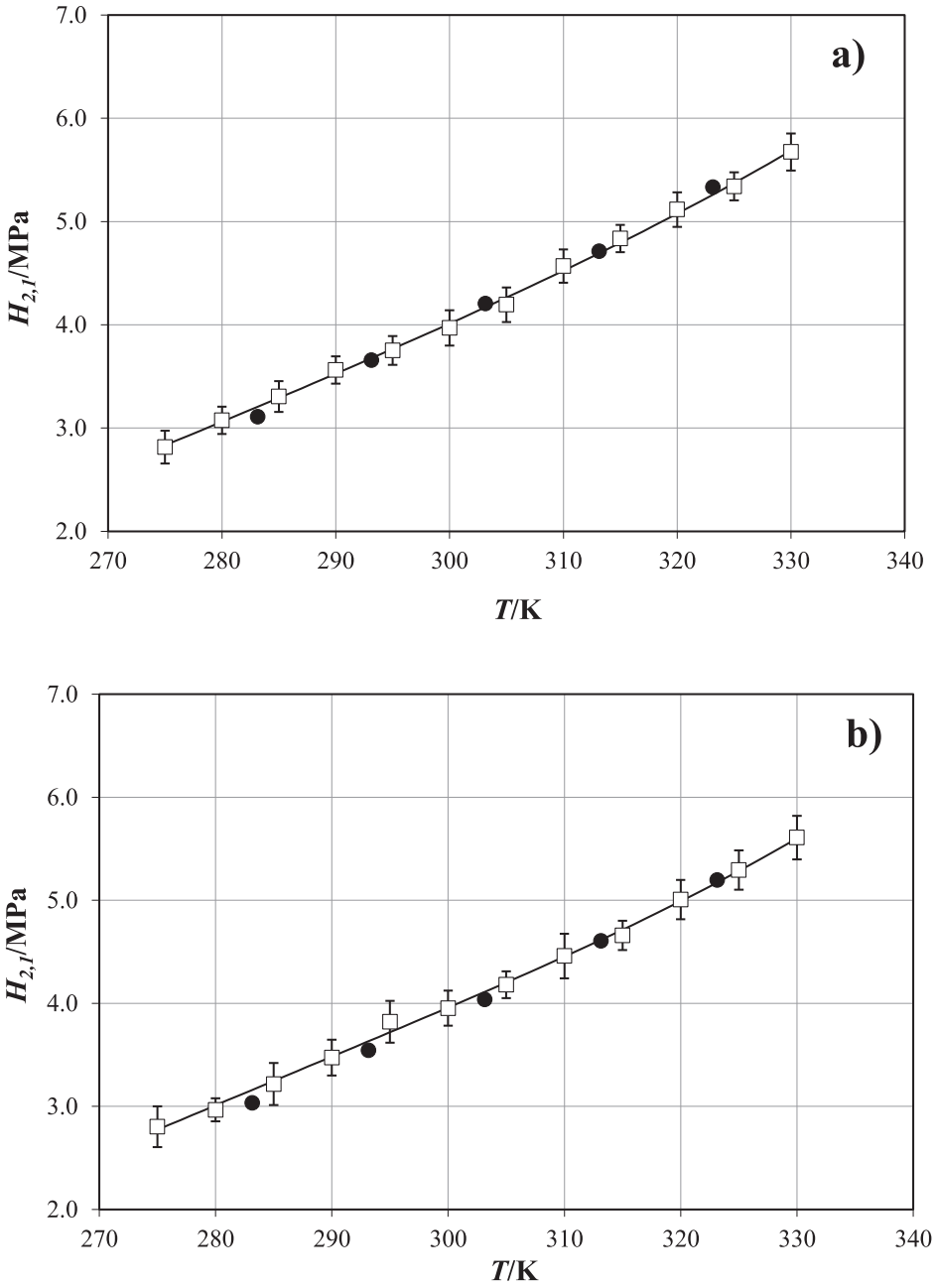

Fig. 1. Henry's constants at 100 kPa, as a function of temperature, for xenon in: *n*-heptane (a), *n*-octane (b) and *n*-nonane (c), *n*-dodecane (d) and *n*-hexadecane (e). Open squares represent the Monte Carlo simulation results (along their error bars), and circles the experimental results from Pollack et al. [20]. The lines are fits using the Clarke and Glew equation.

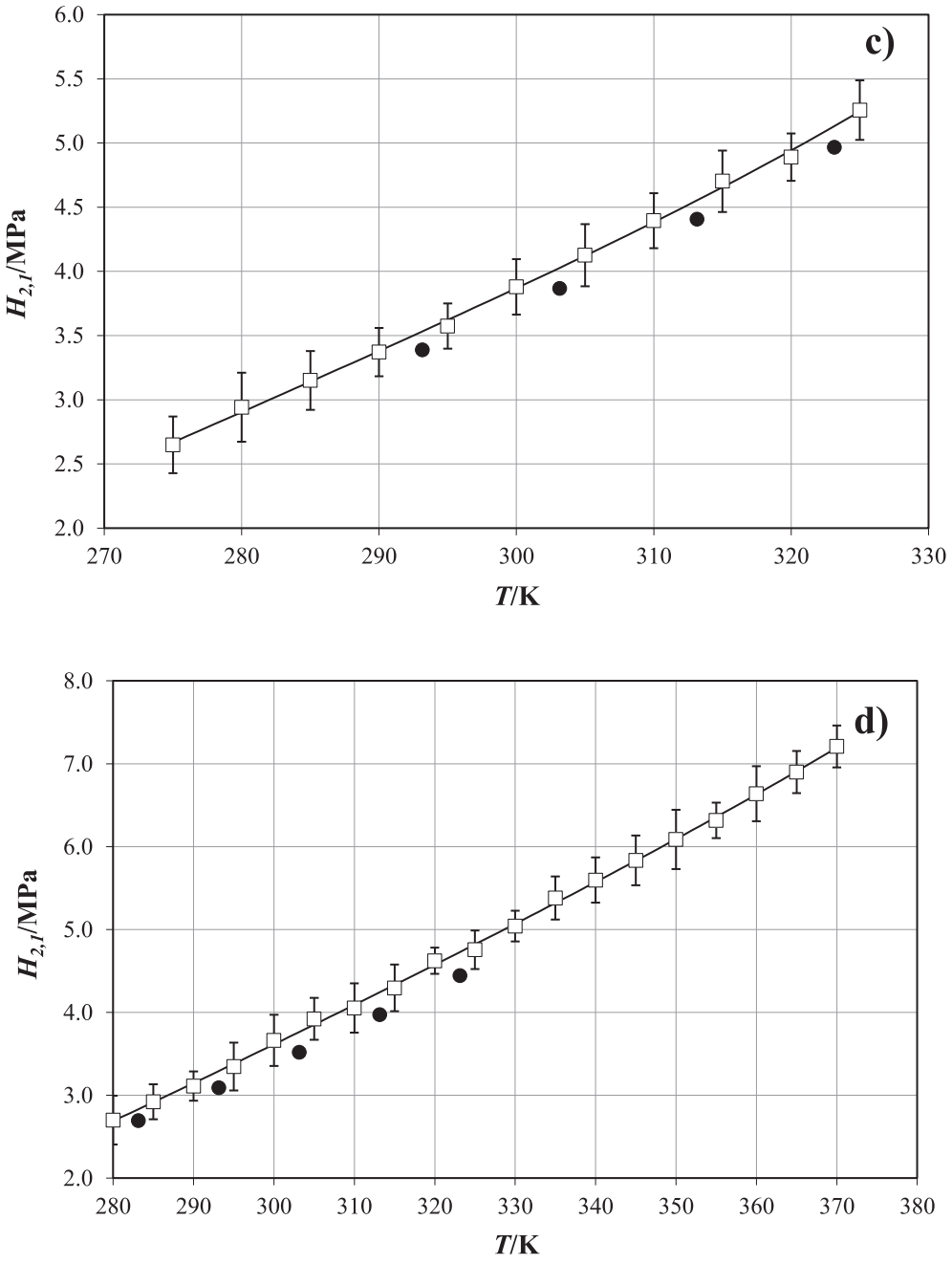

Fig. 1 (*continued*)

standard analytic tail corrections applied to energy and pressure. Temperature and pressure were controlled by using the Nosé-Hoover thermostat (τ_T = 0.5 ps) and Parrinello-Rahman barostat (τ_P = 2.0 ps) respectively, with all bonds constrained to their equilibrium values by the LINCS algorithm [45]. Radial distribution functions were obtained from the production trajectories using the GROMACS *g_rdf* (*gmx rdf*) tool and the calculation was done at a single and different temperature for each system, corresponding to approximately the same experimental reduced temperature of the solvent. In the case of solute–solvent interactions energies, the calculations were done as a function of temperature in essentially the same range as Henry's constant determinations and also at 5 K intervals.

3. Results and discussion

The results obtained from the Monte Carlo simulations for Henrýs constant as a function of temperature are presented in Tables 2 And 3 (for xenon in *n*-alkanes and cycloalkanes, respectively), and plotted in Fig. 1 (xenon in *n*-alkanes) and 2 (xenon in cycloalkanes), along with experimental results from Pollack *et al* [20,21] and Bonifácio *et al* [23,33].

As can be seen, the simulations fully reproduce, within their statistical uncertainties, the Henry's constants of xenon in all the *n*-alkanes and cycloalkanes studied, as was found for *n*-pentane and *n*-hexane in a previous work [23]. This confirms that the solubility of xenon in *n*-alkanes, cyclopentane and cyclohexane can be

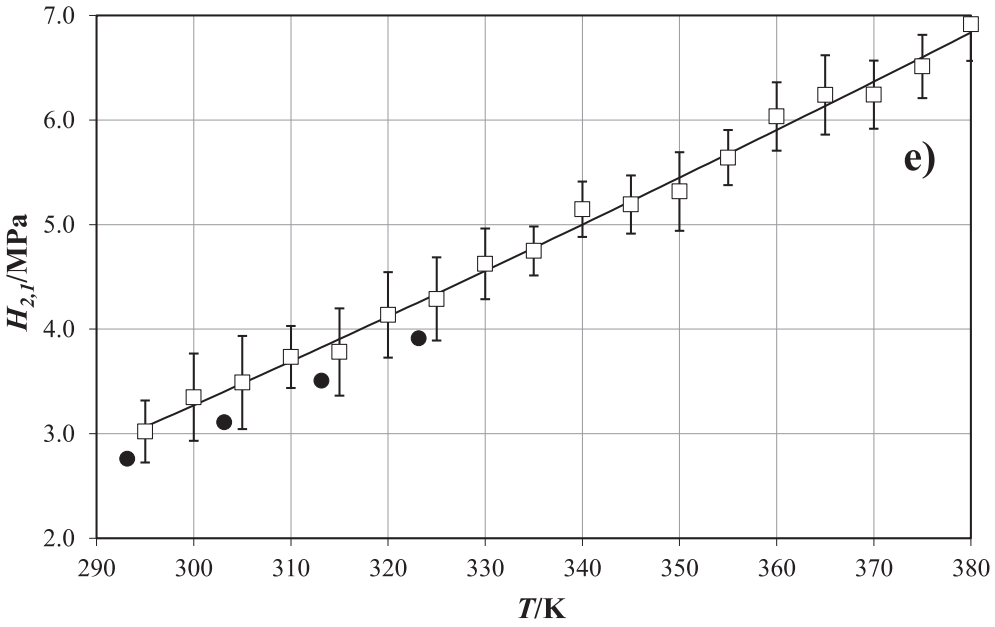

Fig. 1 (*continued*)

predicted quantitatively using the molecular models and simulation methodology (Monte Carlo simulation of the solvent with Widom insertion of the solute) described. Moreover, it should be stressed that these results are achieved using simple Lorentz-Berthelot combining rules, without resorting to fitting any binary parameter to the properties of mixtures.

For xenon in *n*-alkanes, both experimental and simulation values of Henry's constants are quite similar for all the *n*-alkanes, though slightly decreasing as the *n*-alkane chain length grows. This means that, on a mole fraction basis, and compared at the same temperature, the solubility of xenon in *n*-alkanes increases as the solvent chain length increases. However, given the large differences in the chain length of the studied solvents, this analysis may not be the most informative, in part because, at the same absolute temperature, the *n*-alkanes studied are in very different thermodynamic states. Taking this fact into account, Fig. 3 represents the same Henry's constants as a function of the solvent's reduced temperature (results for *n*-pentane and *n*-hexane from Bonifácio *et al* [23] are also included) and a different trend is observed.. At the same reduced temperature, the solubility of xenon in *n*-alkanes now decreases as the chain length increases. For a further comparison, Fig. 4 also shows the solubility of xenon in *n*-alkanes, but now expressed in molar density (moles of solute per volume of solvent) instead of mole fraction. In this representation, it can be observed that the solubility of xenon increases as the solvent chain length decreases, following the decreasing fraction of methyl groups in the solvent molecule.

The same trend of solubility decreasing with chain length is also observed in the cycloalkanes studied (Fig. 5), even though these compounds are constituted only by methylene groups. In this case, this effect can be related to the stronger interaction of xenon with the more hindered cyclic alkanes, as will be discussed further down.

In order to correlate the obtained values of Henry's constants as a function of temperature with a smoothed analytical representation, these were fitted to the equation proposed by Clarke and Glew [46] (3):

$$\ln[H_{2,1}(T,p)/Pa] = A_0 + \frac{A_1}{10^{-2}T/K} + A_2\ln\left(10^{-2}T/K\right) + A_3\left(10^{-2}T/K\right) + A_4\left(10^{-2}T/K\right)^2 + \ldots \quad (3)$$

The four parameter version was used and the fitting curves are plotted in Figs. 1 and 2 while the parameters obtained are presented in table 4. Using this relation for the temperature dependence of Henry's constants, the standard enthalpy of solvation was calculated for all the systems studied as a function of temperature, by equation (4) , and considering p^0 = 100 kPa.

$$\Delta H_2^0(T,p^0) = -RT^2\frac{d}{dT}\left\{\ln\left[\frac{H_{2,1}(T,p^0)}{p^0}\right]\right\} \quad (4)$$

The obtained enthalpies of solvation of xenon in *n*-alkanes are shown in Fig. 6 and those of xenon in cycloalkanes are shown in Fig. 7 in comparison with their linear counterparts (same number of carbon atoms). Also included in the Fig. 6 are the experimental results for xenon in *n*-pentane and *n*-hexane [23] and experimental results for the remaining *n*-alkane systems from Pollack *et al* [20]. In Fig. 7, the enthalpy of solvation of xenon in cyclopentane and cyclohexane from experimental results [21,33] are also included.

In these figures, it can be seen that the enthalpies of solvation of xenon in *n*-alkanes obtained by simulation essentially agree with those from experiment, even noting that Pollack *et al* assumed their values as constant over the temperature range studied. For all the studied *n*-alkanes, including *n*-pentane and *n*-hexane from a previous work, the results lead to the general conclusion that there is a maximum in the ΔH_2^0 *vs. T* curve. This observation is true even though the results for *n*-pentane and *n*-hexadecane do not show an unequivocal maximum in the explored temperature range. The temperatures corresponding to the maxima in ΔH_2^0 for all the systems studied are reported in table 5. Representing solvation enthalpy as a function of solvent's reduced temperature (also in Fig. 6 and table 5), it can be seen that the maxima are located in a relatively narrow temperature range, between 0.51 and 0.56 for all *n*-alkanes studied in this work and also for the dissolution of

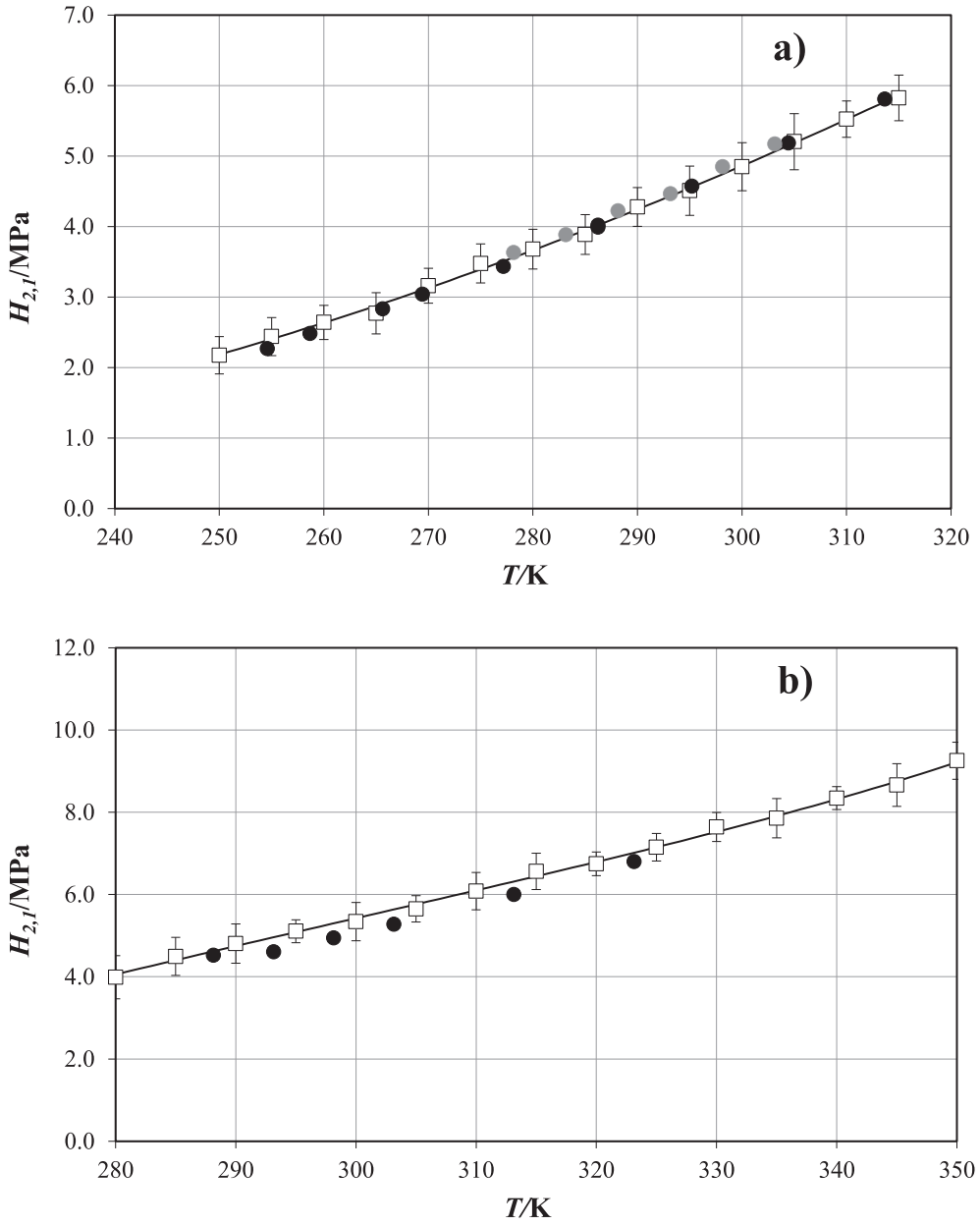

Fig. 2. Henry's constants at 100 kPa, as a function of temperature, for xenon in: cyclopentane (a) and cyclohexane (b). Open squares represent the Monte Carlo simulation results (along their error bars), and circles the experimental results from Bonifácio et al. [33] (black) and Pollack [21] (gey) for cyclopentane and Pollack et al. [21] for cyclohexane. The lines are fits using the Clarke and Glew equation.

xenon in *n*-pentane and *n*-hexane. Moreover, this reduced temperature range where $\frac{d\Delta H_2^0}{dT}$ changes its sign is also very close to the reduced temperature where the mixing process for binary mixtures of *n*-alkanes and of light *n*-alkanes with xenon changes from endothermic to exothermic [17].

In the case of cycloalkanes, the enthalpy of solvation of xenon is generally less negative than in their linear counterparts. For xenon in cyclopentane the simulation results are very close to those obtained from experiment [33] and seem to confirm the inexistence of any maximum in the ΔH_2^0 *vs. T* curve. Moreover, the simulation results for this system also show that ΔH_2^0 increases with temperature (positive $C_{P,0}^2$) in a monotonous fashion, contrarily to what happens for xenon in *n*-pentane where the solvation enthalpy clearly decreases with temperature (negative $C_{P,0}^2$) in most of the temperature range studied. This behavior can be interpreted in the light of Patterson's condensation effect of one flexible or polarizable molecule sticking on a hindered cyclic structure [34–36], an effect that is counteracted by the thermal agitation. In the case of cyclohexane, our calculations show a maximum in ΔH_2^0 at a higher reduced temperature than for *n*-alkanes, but unfortunately the available experimental results do not have a wide enough temperature range or precision to confirm this characteristic. In most of the temperature range considered, the enthalpy of solvation of xenon is more negative in cyclopentane than in cyclohexane, also supporting the above discussed favourable interaction of xenon with the shorter, more hindered cycloalkanes, as was also observed directly on the solubilities.

In order to deepen the discussion about the relative affinity between xenon and each solvent, the solute–solvent interaction

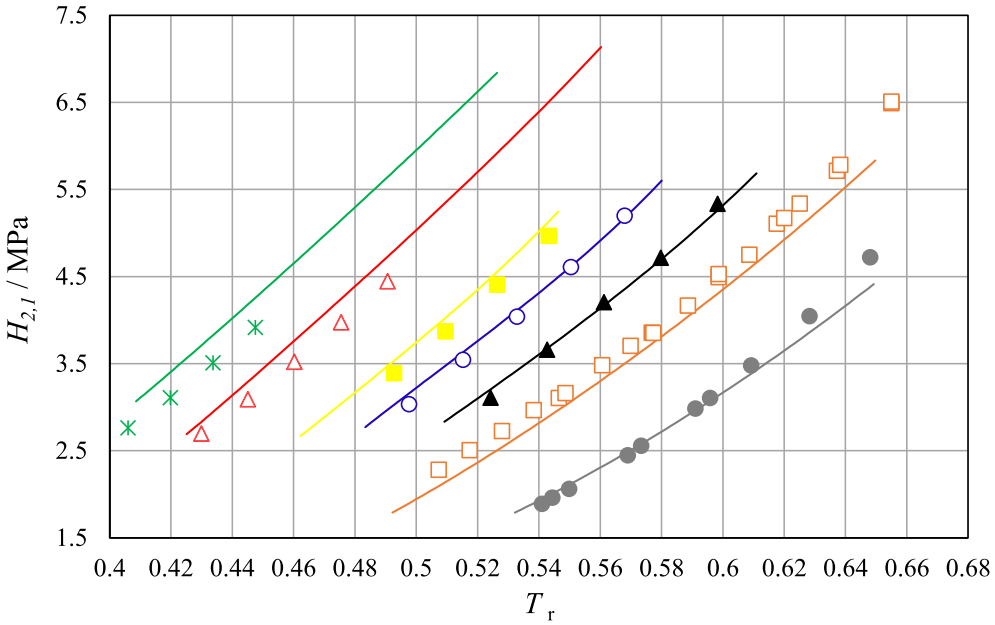

Fig. 3. Henry's constants at 100 kPa as a function of solvent's reduced temperature for xenon in *n*-pentane (grey filled circles), *n*-hexane (orange open squares), *n*-heptane (black filled triangles), *n*-octane (blue open circles), *n*-nonane (yellow filled squares), *n*-dodecane (red open triangles) and *n*-hexadecane (green crosses). Symbols: experimental results (ref. 20 and 23); lines, simulation results (ref. 20 and this work).

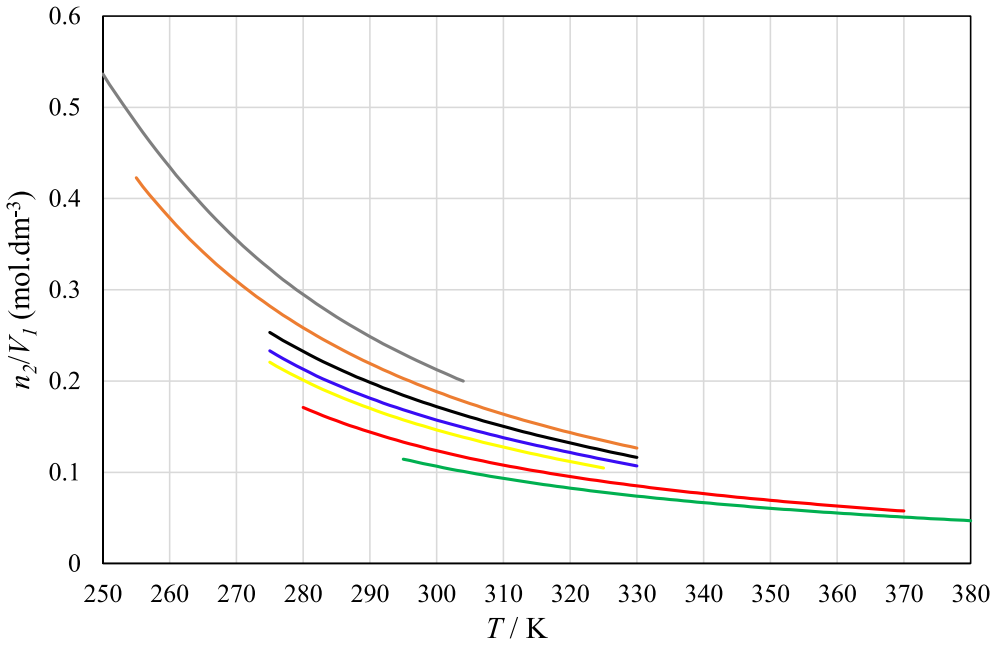

Fig. 4. Smoothed curves for the solubility of xenon in *n*-alkanes (in moles of solute per volume of solvent) at 100 kPa as a function of temperature obtained by Monte Carlo simulations. The same colour code as Fig. 3.

energies were obtained from molecular dynamics simulations for all the systems studied (including xenon in *n*-pentane and xenon in *n*-hexane). Figs. 8 and 9 show the smoothed curves obtained for the solute–solvent interaction energy (E_{int}) both as a function of temperature (a) and as a function of the solvent's reduced temperature (b).

First, it can be observed that the interaction energies increase linearly with temperature for all the systems studied. For the *n*-alkanes (Fig. 8), these lines are parallel to each other, revealing a similar behaviour with temperature, since the lines can be almost superimposed by a mere temperature translation. At a given temperature, the interaction energy decreases (becomes more negative) when the solvent chain length increases but, as was observed for the solvation enthalpy, this trend is inverted when the solvents are compared at the same reduced temperature.

For the cycloalkane systems (Fig. 9), it is seen that the interaction energy between xenon and the solvent is more negative for cyclohexane than for cyclopentane, and that this trend remains when the energy values are represented as a function of the solvent's reduced temperature. This fact can be due to a higher

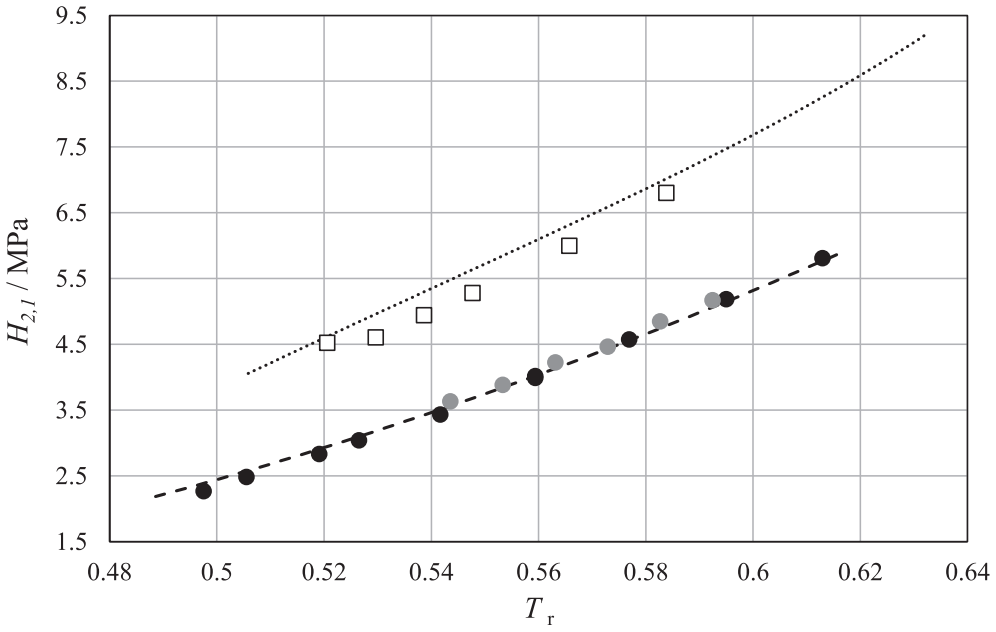

Fig. 5. Henry's constants at 100 kPa for xenon in cyclopentane (filled circles) and cyclohexane (open squares) as a function of solvent's reduced temperature. Symbols: experimental results (ref. 21 – grey symbols and 33 – black symbols); lines (dashed for cyclopentane and dotted for cyclohexane), simulation results (this work).

Table 4
Coefficients of equation (3) fitting simulated data for xenon in *n*-heptane, *n*-octane and *n*-nonane, *n*-dodecane, *n*-hexadecane, cyclopentane and cyclohexane.

	A_0	A_1	A_2	A_3	AAD (%)
Xenon in *n*-heptane	109.28	−134.56	−82.05	13.64	0.69
Xenon in *n*-octane	198.67	−256.72	−162.10	26.73	0.41
Xenon in *n*-nonane	165.68	−212.01	−132.22	21.81	0.62
Xenon in *n*-dodecane	71.23	−83.77	−42.59	6.197	0.70
Xenon in *n*-hexadecane	42.97	−44.90	−18.63	2.487	1.64
Xenon in cyclopentane	28.08	−23.79	−7.727	1.246	1.03
Xenon in cyclohexane	164.45	−210.38	−126.00	19.87	1.05

diversity of the solute–solvent interaction orientation in the case of cyclohexane. The same figure also shows that, for the same number of carbon atoms, xenon presents a more favourable (negative) interaction energy with cycloalkanes than with *n*-alkanes.

A clearer picture of the behaviour of the solute–solvent interaction energy in this kind of systems can be obtained by representing this property as a function of solvent carbon molar density (in an analogous fashion as in reference 27), in order to take into account the different thermodynamic state where each solvent is found at each temperature. This representation is shown in Fig. 10 and, as can be seen, for the same (or close) values of abscissa, the solute–solvent interaction energy is more negative for the shorter *n*-alkanes, which have the highest proportion of the more interactive methyl groups. Concerning the behaviour of xenon in cycloalkanes, there are two conclusions that can be drawn: 1) the interaction energies are less negative than those of *n*-alkanes, in line of what would be expected of alkanes formed solely by the less interactive methylene groups; 2) the interaction energies for cyclopentane are more negative than for cyclohexane: being both solvent molecules constituted only by CH_2 units, the more hindered structure of cyclopentane must play an important role in the interactions with the solute, probably contributing to expose more efficiently the interactive groups to xenon.

The liquid structure of the model systems studied was probed by the calculation of radial distribution functions [rdf, $g(r)$]. These were obtained from the molecular dynamics trajectories of solutions of xenon in *n*-pentane, *n*-hexane, *n*-heptane, *n*-octane, *n*-nonane, *n*-dodecane, *n*-hexadecane, cyclopentane and cyclohexane, at different absolute temperatures (respectively 250, 260, 280, 295, 305, 340, 370, 260 and 285 K) corresponding to a similar (in the range 0.51–0.53) reduced temperature for each solvent. In the following analysis, the CH_2 atoms bonded to a CH_3 atom are designated C2, those bonded to a C2 are designated C3 and so on.

The results of $g(r)$ for CH_3 and CH_2 around xenon atoms are shown in Fig. 11 [a) to f)] for (xenon + *n*-alkane) systems. As can be seen, the first peak for Xe/CH_3 is the most intense in all systems, appearing at lower distances than any of the CH_2 peaks. This observation agrees with the aforementioned tendency of xenon to dissolve near the methyl groups of *n*-alkanes. The height of this first Xe/CH_3 peak is quite similar for the shorter solvents (*n*-pentane to *n*-nonane), showing only a slight increasing trend with chain length. The two longest solvents, however, present a different structure, with significantly higher CH_3/CH_3 and Xe/CH_3 first peaks; these longer *n*-alkanes seem to present a higher tendency for the methyl groups to cluster together, creating cavities where xenon preferentially dissolves. The differences in liquid structure between the shorter and the longer alkanes are evidenced by the Xe/CH_2 radial distribution functions: for each solvent up to *n*-nonane, all the Xe/CH_2 first peaks maxima are higher than 1.4 and appear at essentially the same distance of ca. 0.48 nm, with the C2 methylene groups presenting a higher intensity than the

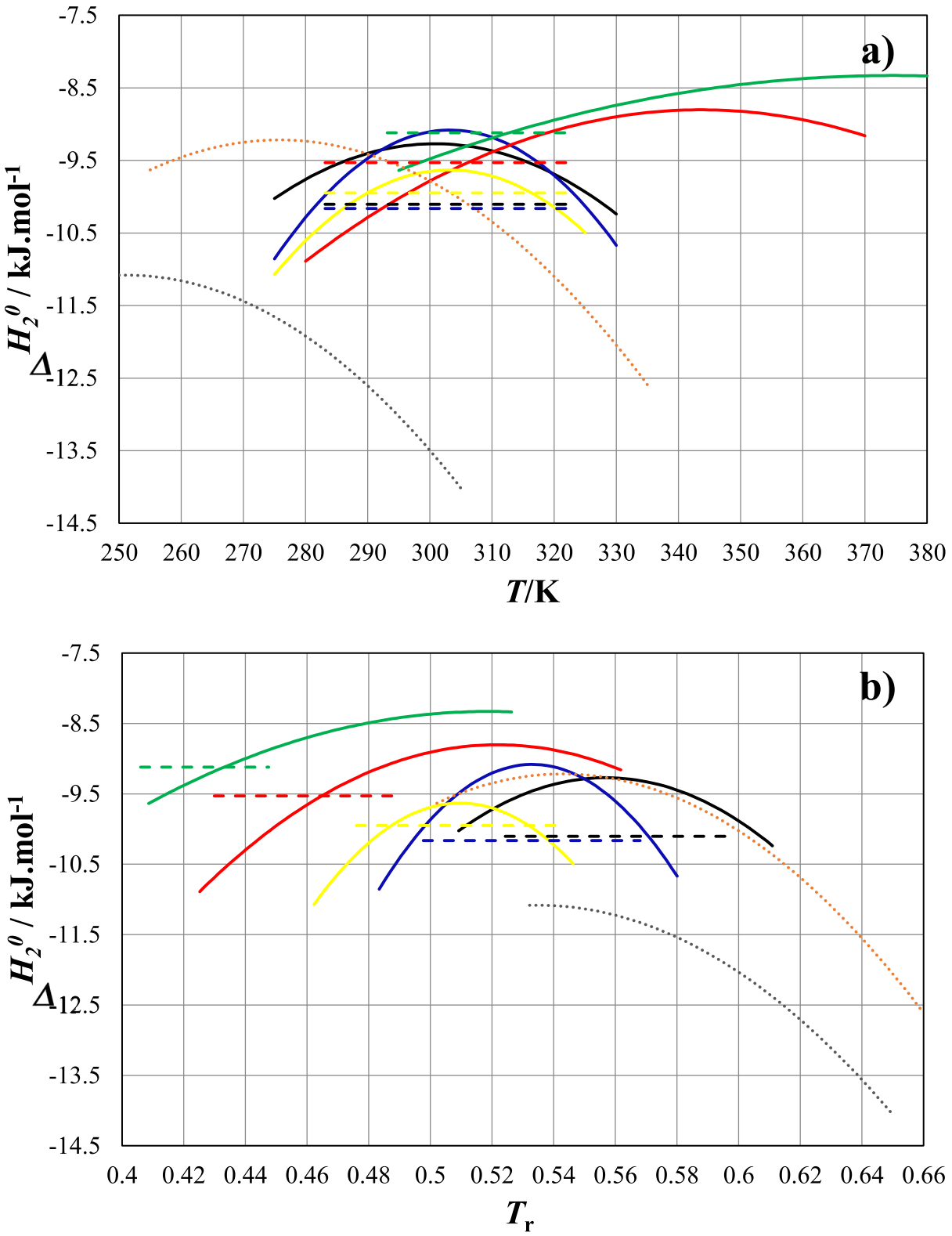

Fig. 6. Standard enthalpy of solvation for xenon in *n*-heptane (black), *n*-octane (blue), *n*-nonane (yellow), *n*-dodecane (red) and *n*-hexadecane (green) as a function of temperature (a) and solvent's reduced temperature (b) from simulation results of this work (solid lines) and experiment from reference 20 (dashed lines). Experimental results of xenon in *n*-pentane (grey) and *n*-hexane (orange) reference 23 are also included as dotted lines.

others. In the shorter solvents, xenon is preferentially solvated near the methyl groups, but is able to contact/collide frequently with all the remaining methylene groups. The longer *n*-alkanes present a different solvation behavior: besides the much higher Xe/CH_3 peaks, the first maxima of all the Xe/CH_2 radial distribution functions (at ca. 0.45 nm, showing as a shoulder for C2 and C3) are now much less intense and lower than 1; moreover, the highest peak for each Xe/CH_2 $g(r)$ now appears at a length that increases

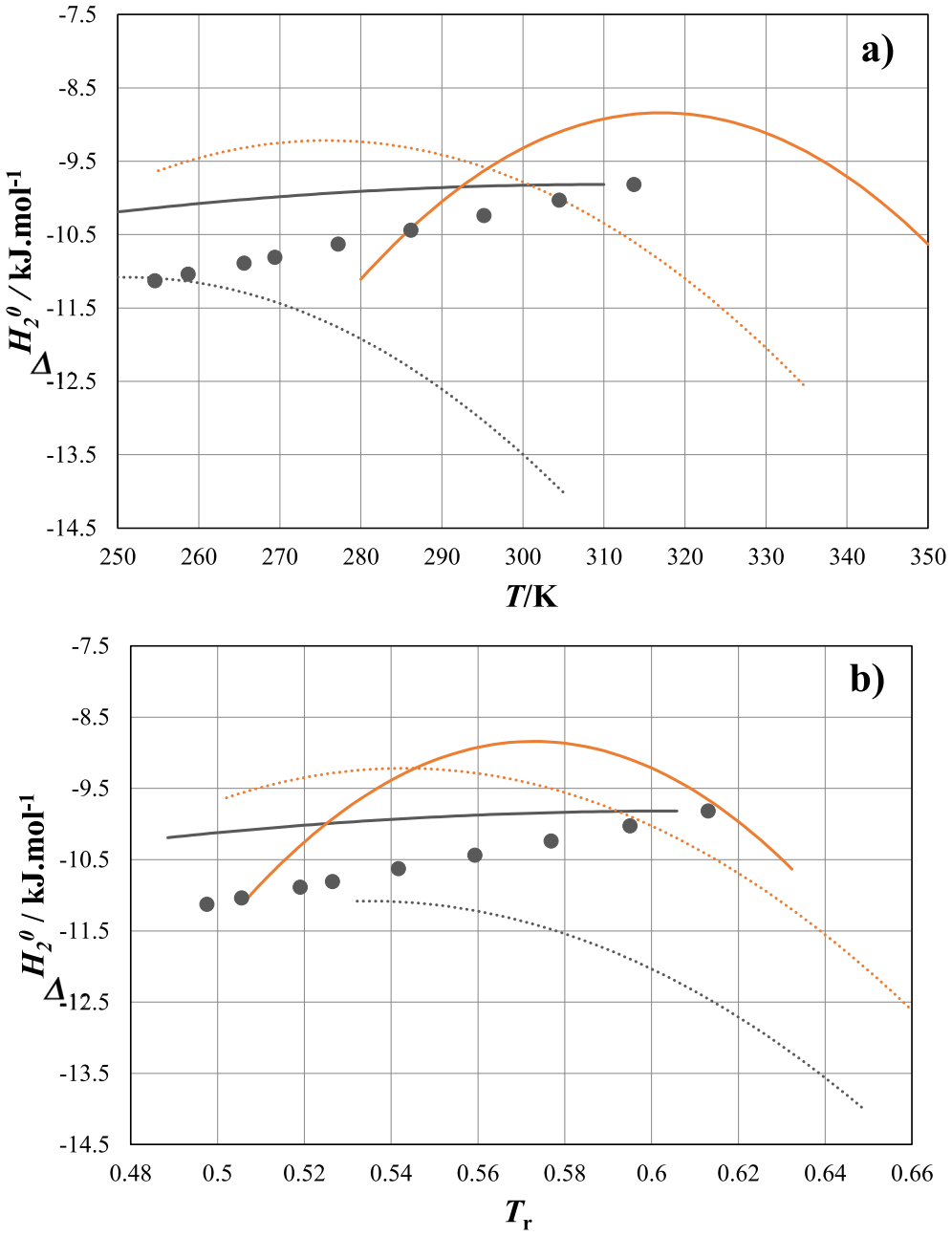

Fig. 7. Standard enthalpy of solvation for xenon in cyclopentane (full grey line) and cyclohexane (full orange line) as a function of temperature (a) and solvent's reduced temperature (b) from simulation results in comparison with the same property for xenon in *n*-pentane and *n*-hexane (same color code as Fig. 6). Filled grey circles: enthalpy of solvation of xenon in cyclopentane from experimental results [33].

Table 5
Temperatures for which the enthalpy of solvation of xenon in each solvent reaches its maximum value, along with the corresponding solvent's reduced temperature (calculated from the experimental critical temperatures of the solvents).

Solvent	T (máx. ΔH_2^{θ}) /K	T_r (máx. ΔH_2^{θ})
n-pentane	251.3*	0.534*
n-hexane	275.8*	0.543*
n-heptane	300.8	0.557
n-octane	303.3	0.533
n-nonane	303.7	0.510
n-dodecane	343.6	0.522
n-hexadecane	374.5	0.519
Cyclopentane	–	–
Cyclohexane	317.1	0.573

*Values obtained from experimental results.

commensurately with its distance from the methyl group, meaning that it stems from the Xe/CH_3 interaction. Thus, in the longer *n*-alkanes, xenon can be regarded as being essentially solvated by the CH_3 groups of the solvent and only rarely contacting at a close range with the CH_2 groups (as seen by the first peaks which are much lower than 1).

The tendency of xenon to be solvated by the methyl groups of the *n*-alkane solvents can be quantified by integrating the radial distribution functions, thus obtaining the number of interaction sites (N) of each type in a coordination shell around the reference site as:

$$N = 4\pi \int_{r_1}^{r_2} g(r) r^2 \rho dr \tag{7}$$

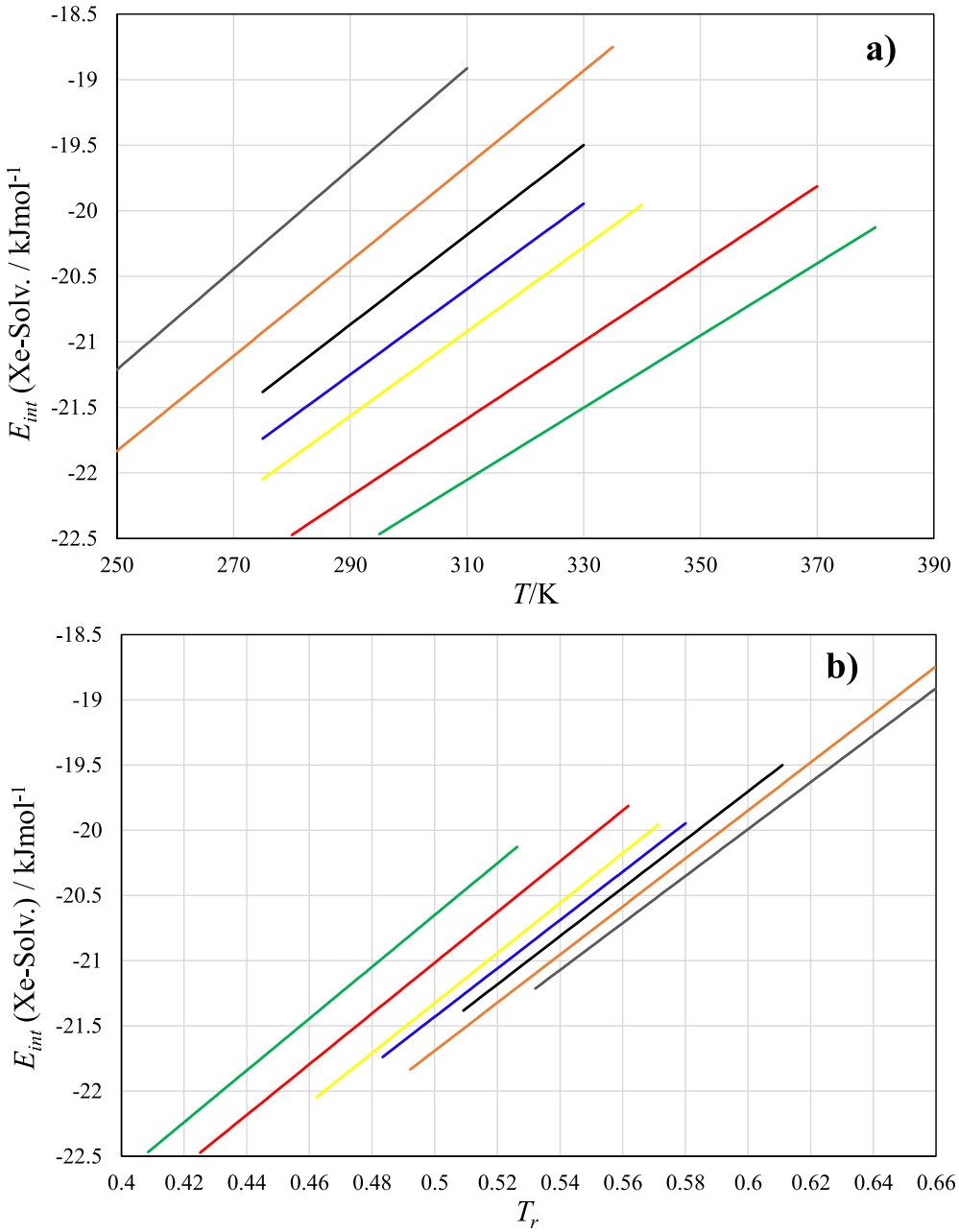

Fig. 8. Solute-solvent interaction energies for xenon in *n*-pentane (grey), *n*-hexane (orange) *n*-heptane (black), *n*-octane (blue), *n*-nonane (yellow), *n*-dodecane (red), *n*-hexadecane (green), as a function of temperature (a) and solvent's reduced temperature (b) from simulation results of this work. Statistical uncertainties for energies: from 0.050 kJmol^{-1} for xenon in *n*-pentane to 0.067 kJmol^{-1} for xenon in *n*-octane and xenon in *n*-nonane.

where r_1 and r_2 are the inner and outer radii of the coordination shell and ρ is the segment bulk density. Given the uncertainty in defining the limits of the coordination sphere, we have calculated the number of sites of a given group around xenon, as a function of the distance from its centre. From these data, the ratio between the local molar fraction of CH_3 groups around xenon and their bulk molar fraction, as a function of the radius r of the coordination sphere has been calculated for all the systems and shown in Fig. 12. As can be seen, the fraction of CH_3 groups is always higher than the bulk value at low r, tending to the bulk value for large r, which is a clear indication of an enrichment phenomenon of CH_3 around xenon. Moreover, the ratio $\times$ (CH_3) / x $(CH_3)_{bulk}$ increases with the increasing chain length of the solvent, showing that the enrichment of methyl groups around xenon at short distances is more pronounced for the longest *n*-alkanes. That trend is particularly apparent in the case of *n*-dodecane and *n*-hexadecane and follows the results found by Morgado *et al* [25] for *n*-butane, *n*-hexane, *n*-undecane and *n*-hexadecane using a different force field (OPLS-AA).

The $g(r)$ results obtained for the (xenon + cycloalkane) systems are shown in Fig. 13 a), where it can be seen that the two solvents studied display very different structural behaviors, despite being constituted only by the same CH_2 chemical groups. The different structure of the two solvents is evident from the CH_2-CH_2 rdf, which is much more structured in the case of cyclopentane, displaying three clear peaks, whereas cyclohexane shows a broad first band covering a wide variety of distances. The structural differences are also reflected in the rdf with xenon: despite "lifting-

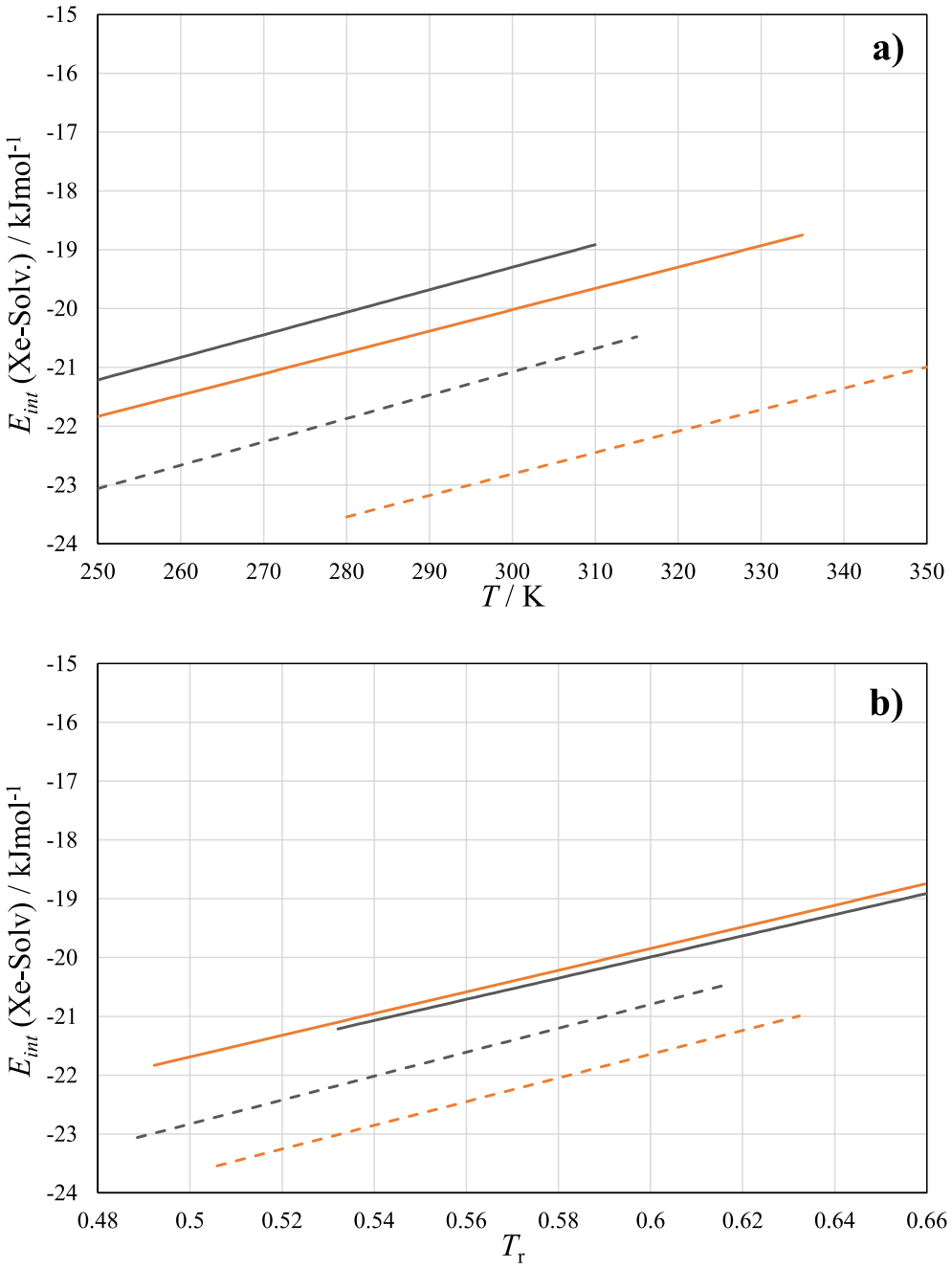

Fig. 9. Solute-solvent interaction energies for xenon in cyclopentane (dashed grey) and cyclohexane (dashed orange) as a function of temperature (a) and solvent's reduced temperature (b) from simulation results of this work, in comparison with those for xenon in *n*-pentane (full grey) and *n*-hexane (full orange). Statistical uncertainties for energies: 0.046 kJmol^{-1} for xenon in cyclopentane to 0.082 kJmol^{-1} for xenon in cyclohexane.

off" at a shorter distance, the Xe-CH_2 $g(r)$ in cyclohexane shows a broad first peak with a long "tail" towards larger values of r, whereas cyclopentane displays a quite intense first peak with two clear shoulders at higher r. This should be due to the different molecular structures of two solvents. The flexibility of cyclohexane (with more energetically accessible conformations) tends to smear out the different orientations of xenon/CH_2 and CH_2/CH_2 interactions, leading to broad peaks in $g(r)$, whereas the higher rigidity of cyclopentane leads a more structured liquid, with a clearer definition of preferential orientations between adjacent molecules, which results in the individualization of the distances involving each methylene unit.

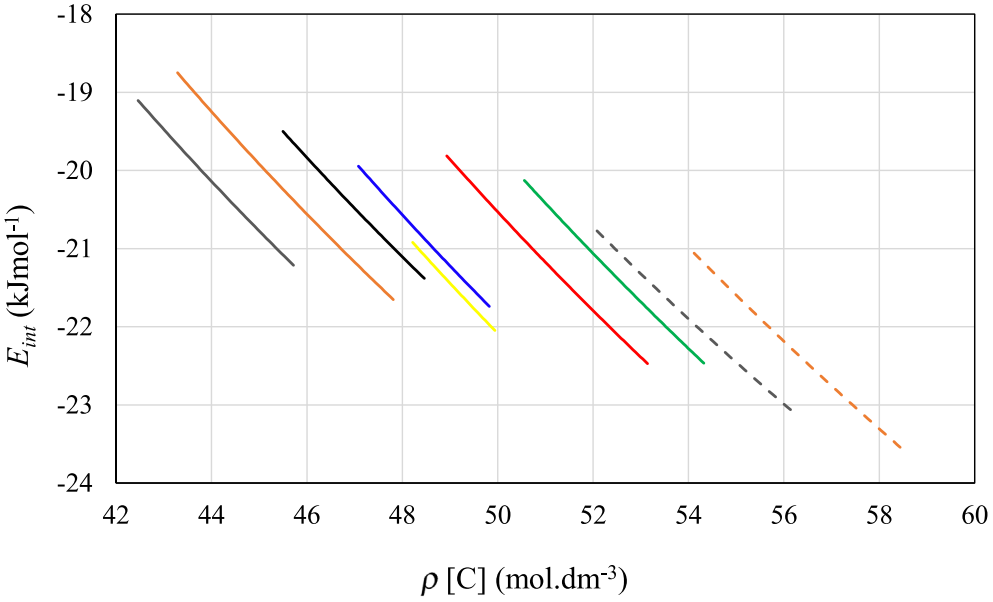

Fig. 10. Solute-solvent interaction energies for xenon in all the studied solvents (including *n*-pentane and *n*-hexane) from simulation results of this work as a function of molar density of carbon atoms. The same colour code as Figs. 8 and 9.

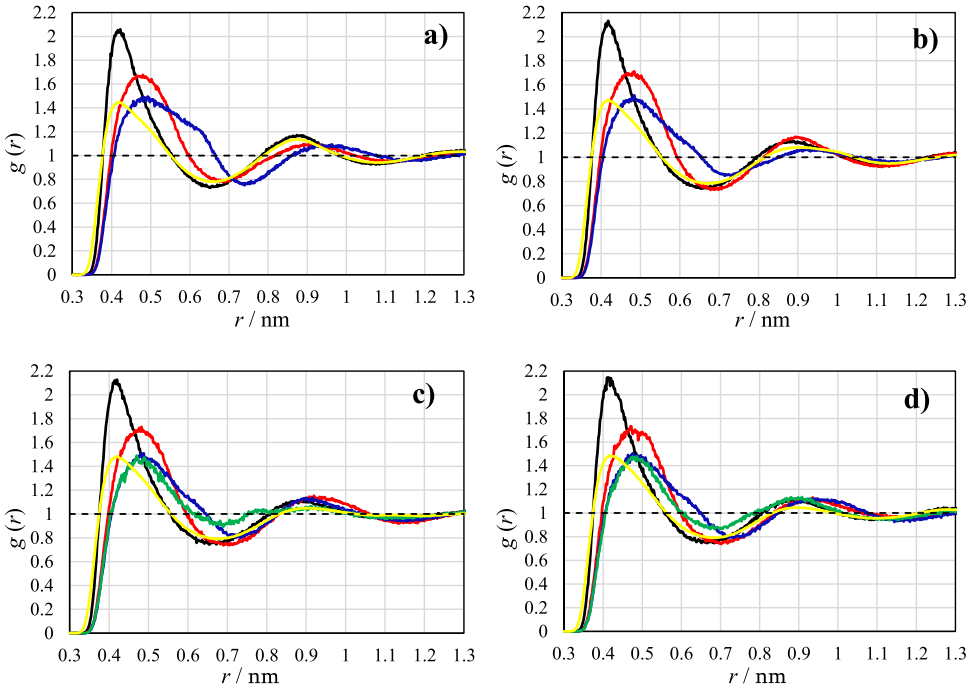

Fig. 11. Radial distribution functions for xenon in *n*-pentane (a), *n*-hexane (b), *n*-heptane (c), *n*-octane (d), *n*-nonane (e), *n*-dodecane (f), and *n*-hexadecane (g) at 250, 260, 280, 295, 305, 340 and 370 K, respectively. CH_3 (black), C2 (red), C3 (blue), C4 (green), C5 (orange), C6 (violet), C7 (brown), C8 (dark green) around xenon. Yellow lines: CH_3 around CH_3.

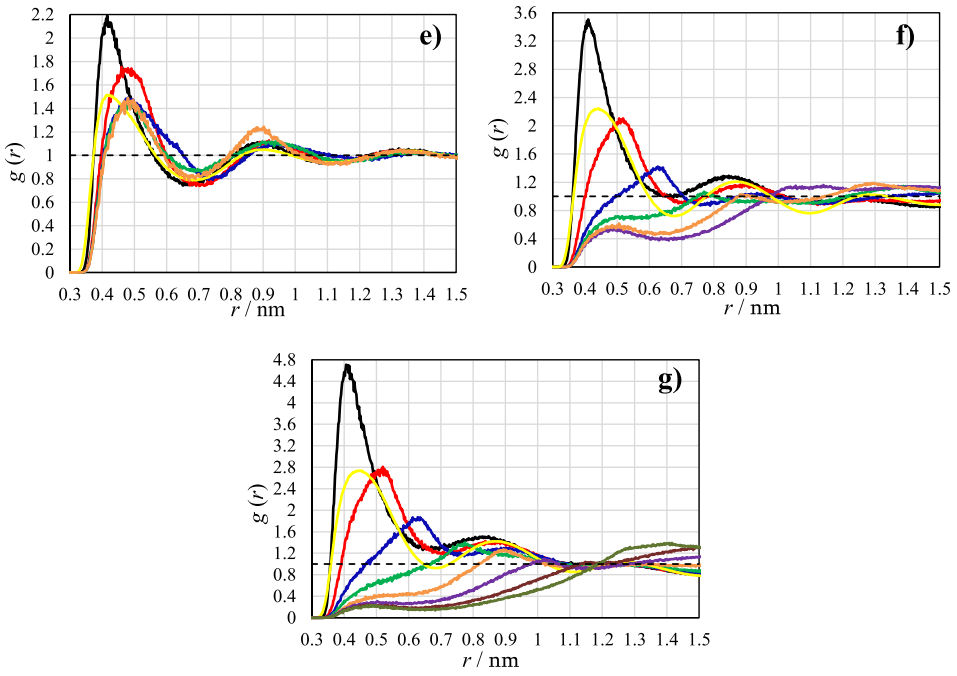

Fig. 11 (*continued*)

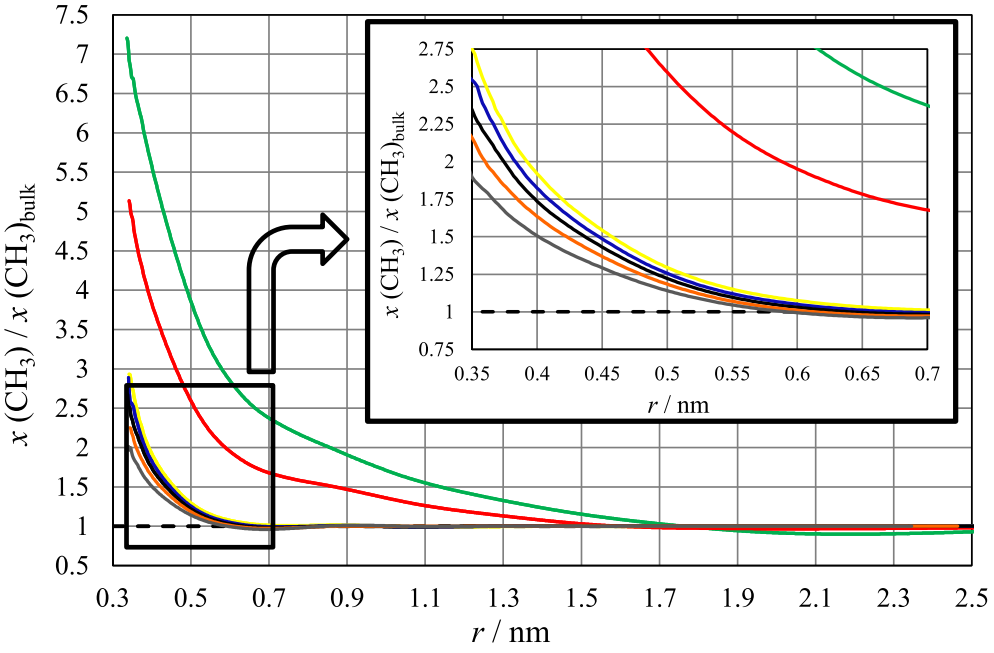

Fig. 12. Ratio between CH_3 local fraction around xenon and bulk CH_3 fraction for xenon in *n*-pentane (grey), *n*-hexane (orange), *n*-heptane (black), *n*-octane (blue), *n*-nonane (yellow), *n*-dodecane (red) and *n*-hexadecane (green). The inset represents a more local view of the figure allowing to distinguish between the curves for the *n*-alkanes with chain lengths between C_5 and C_9.

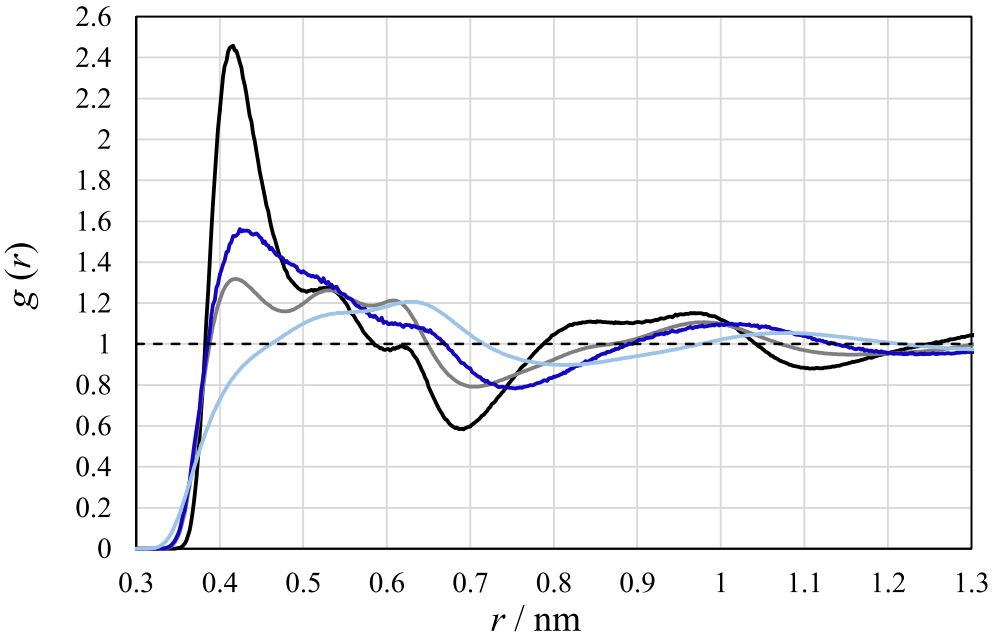

Fig. 13. Radial distribution functions for xenon in cycloalkanes: xenon around CH_2 (black) and CH_2 around CH_2 (grey) for xenon in cyclopentane at 265 K and xenon around CH_2 (dark blue) and CH_2 around CH_2 (light blue) for xenon in cyclohexane at 285 K.

4. Conclusions

Solutions of xenon in *n*-alkanes and cycloalkanes have been studied by computer simulation. *n*-alkanes have been modelled by the united atom TraPPE force field, using the optimized non-bonded parameters considered in a previous work. Cycloalkanes have been modelled using the same force field, with non-bonded parameters obtained in the context of this work. All the optimized parameters were used in a transferable fashion within each family of solvents. For xenon, an optimized potential model based on a simple Lennard-Jones spherical model from Bohn *et al* was used. Using these models and simple Lorentz-Berthelot combining rules, Henrýs constants of xenon in a series of *n*-alkanes (*n*-heptane, *n*-octane, *n*-nonane, *n*-dodecane and *n*-hexadecane) and in two cycloalkanes (cyclopentane and cyclohexane) have been obtained by Monte Carlo computer simulations at a reference pressure and as a function of temperature. A remarkable agreement between the simulation and experimental results of Henry's constants was observed, particularly taking into account the simplicity of the models used and the absence of any fitted binary parameter.

From the temperature dependence of Henry's constants, standard enthalpies of solvation for all the systems as a function of temperature were calculated, for which an excellent agreement with the available experimental results was obtained. The singularity of the standard enthalpy results (a maximum in the ΔH_2^0 *vs. T* curve) for xenon in *n*-alkanes was found to be regular within the *n*-alkane series, since it occurred nearly at the same solvent's reduced temperature for all the systems (between 0.51 and 0.55). The solute–solvent interaction energies were also obtained by molecular dynamics simulations using the same models and showed a linear dependence with temperature for all the systems studied. When compared at both the same temperature and reduced temperature the solute–solvent interaction energies of xenon in cycloalkanes are lower (more negative) than for xenon in *n*-alkanes. The representation of the solute–solvent interaction energies as a function of the molar density of carbon atoms allow unveiling the solvents with higher CH_3 content as more interactive, with xenon being less interactive towards cycloalkanes than towards *n*-alkanes.

The structure of the solutions xenon/solvent was also studied by the calculation of xenon/CH_n and CH_n/CH_n radial distribution functions for all the solvents at nearly corresponding states. The results confirm the enrichment of methyl groups around xenon in comparison with methylene group for *n*-alkanes, being this effect more pronounced for the longest *n*-alkanes. The interaction xenon/CH_2 and CH_2/CH_2 for xenon in cyclopentane seems to be more structured than the corresponding interaction for xenon in cyclohexane, which may be a consequence of the more hindered molecular structure of cyclopentane in comparison with cyclohexane.

CRediT authorship contribution statement

Luís F.G. Martins: Conceptualization, Methodology, Formal analysis, Investigation, Writing - original draft, Validation. **Alfredo J. Palace Carvalho:** Methodology, Software, Validation, Data curation. **Pedro Morgado:** Conceptualization, Methodology, Formal analysis, Writing - review & editing. **Eduardo J.M. Filipe:** Conceptualization, Methodology, Formal analysis, Writing - review & editing.

Declaration of Competing Interest

The authors declare that they have no known competing financial interests or personal relationships that could have appeared to influence the work reported in this paper.

Acknowledgements

LFGM and AJPC acknowledge the financial support from Fundação para a Ciência e Tecnologia by the project POCTI/QUI/46299/2002 and the computational facilities from Instituto de Ciências da Terra (Évora University unit). LAQV-REQUIMTE, Évora pole, acknowledges financial support by National Funds through Fundação para a Ciência e Tecnologia within the scope of the project UIDB/50006/2020.

Centro de Química Estrutural acknowledges financial support from Fundação para a Ciência e Tecnologia (UIDB/00100/2020).

References

[1] P.D. Harris, R. Barnes, The uses of helium and xenon in current clinical practice, Anaesthesia 63 (2008) 284–293.
[2] L.T. Liu, Y. Xu, P. Tang, Mechanistic insights into xenon inhibition of NMDA receptors from MD simulations, J. Phys. Chem. B 114 (2010) 9010–9016.
[3] R. Dickinson, B.K. Peterson, P. Banks, C. Simillis, J.C. Martin, C.A. Valenzuela, M. Maze, N.P. Franks, Competitive inhibition at the glycine site of the N-methyl-D-aspartate receptor by the anesthetics xenon and isoflurane: evidence from molecular modeling and electrophysiology, Anesthesiology 107 (2007) 756–767.
[4] M. Gruss, T.J. Bushell, D.P. Bright, W.R. Lieb, A. Mathie, N.P. Franks, Two-pore-domain K channels are a novel target for the anesthetic gases xenon, nitrous oxide and cyclopropane, Mol. Pharmacol. 65 (2004) 443–452.
[5] R.D. Booker, A.K. Sum, Biophysical changes induced by xenon on phospholipid bilayers, BBA 1828 (2013) 1347–1356.
[6] J. Chen, L. Chen, Y. Wang, X. Wang, S. Zeng, Exploring the effects on lipid bilayer induced by noble gases *via* molecular dynamics simulations, Sci Rep. 5 (2015) 17235.
[7] M. Weinrich, D. Worcester, Xenon and other volatile anesthetics change domain structure in model lipid raft membrane, J. Phys. Chem. B 117 (2013) 16141–16147.
[8] E. Yamamoto, T. Akimoto, H. Shimizu, Y. Hirano, M. Yasui, K. Yasuoka, Diffusive nature of xenon anesthetic changes properties of a lipid bilayer: molecular dynamics simulations, J. Phys. Chem. B 116 (2012) 8989–8995.
[9] J.S. Rowlinson, F.L. Swinton, Liquids and liquid mixtures, 3rd ed., Butterworths, 1982.
[10] J.R. Mick, M.S. Barhaghi, B. Jackman, K. Rushaidat, L. Schwiebert, J.J. Potoff, Optimized Mie potentials for phase equilibria: application to noble gases and their mixtures with *n*-alkanes, J. Chem. Phys. 143 (11) (2015) 114504.
[11] A.B. Pereiro, M.J. Pastoriza-Gallego, K. Shimizu, I.M. Marrucho, J.N. Canongia Lopes, M.M. Piñeiro, L.P.N. Rebelo, On the formation of a third, nanostructured domain in ionic liquids, J. Phys. Chem. B 117 (2013) 10826–10833.
[12] P. Morgado, A.R. Garcia, L.F.G. Martins, L.M. Ilharco, E.J.M. Filipe, Alkane coiling in perfluoroalkane solutions: a new primitive solvophobic effect, Langmuir 33 (2017) 11429–11435.
[13] P. Fontaine, L. Bardin, M.C. Fauré, E.J.M. Filipe, M. Goldmann, Evidence of lying molecules in the structure of the most condensed phase of semi-fluorinated alkane monolayers, Nanoscale 10 (2018) 2310–2316.
[14] E.J.M. Filipe, E.J.S. Gomes de Azevedo, L.F.G. Martins, V.A.M. Soares, J.C.G. Calado, C. McCabe, G. Jackson, Thermodynamics of liquid mixtures of xenon with alkanes: (xenon + ethane) and (xenon + propane), J. Phys. Chem. B 104 (6) (2000) 1315–1321.
[15] L.F.G. Martins, E.J.M. Filipe, J.C.G. Calado, C. McCabe, G. Jackson, Thermodynamics of liquid mixtures of xenon with alkanes: (xenon + *n*-butane) and (xenon + Isobutane), J. Phys. Chem. B 104 (6) (2000) 1322–1325.
[16] L.F.G. Martins, E.J.M. Filipe, J.C.G. Calado, Thermodynamics of liquid mixtures involving cyclic molecules. 2: xenon + cyclobutane, J. Phys. Chem. B 105 (44) (2001) 10936–10941.
[17] L.F.G. Martins, A.J. Palace Carvalho, J.P. Prates Ramalho, E.J.M. Filipe, Excess thermodynamic properties of mixtures involving xenon and light alkanes: a study of their temperature dependence by computer simulation, J. Phys. Chem. B 115 (32) (2011) 9745–9765.
[18] L.M.B. Dias, C. McCabe, E.J.M. Filipe, J.C.G. Calado, Thermodynamics of liquid (xenon + methane) in the critical region, J. Phys. Chem B 108 (2004) 7377–7381.
[19] R.P. Bonifácio, A.A.H. Pádua, M.F. Costa-Gomes, C. McCabe, E.J.M. Filipe, Predicting the solubility of xenon in *n*-hexane and *n*-perfluorohexane, Mol. Phys. 100 (2002) 2547–2553.
[20] G.L. Pollack, J.F. Himm, Solubility of xenon in liquid *n*-alkanes: temperature dependence and thermodynamic functions, J. Chem. Phys. 77 (1982) 3221–3229.
[21] G.L. Pollack, R.P. Kennan, J.F. Himm, Solubility of xenon in 45 organic solvents including cycloalkanes, acids and alkanals: experiment and theory, J. Chem. Phys. 90 (1989) 6569–6579.
[22] R.P. Bonifácio, M.F. Costa Gomes, E.J.M. Filipe, Solubility of xenon in *n*-hexane between 257 and 333 K, Fluid Phase Equilib. 193 (2002) 41–45.
[23] R.P.F. Bonifácio, L.F.G. Martins, C. McCabe, E.J.M. Filipe, On the behavior of solutions of xenon in liquid *n*-alkanes: solubility of xenon in *n*-pentane and *n*-hexane, J. Phys. Chem. B 114 (2010) 15897–15904.
[24] E.J.M. Filipe, L.M.B. Dias, J.C.G. Calado, C. Clare McCabe, G. George Jackson, "Is xenon an ennobled alkane?, Phys Chem. Chem. Phys. 4 (2002) 1618–1621.
[25] B.L. Eggimann, B. L.; Sunnarborg, A. J.; Stern, H. D.; Bliss, A. P.; J. I. Siepmann, J. L., "An Online Parameter and Property Database for the TraPPE Force Field", Mol. Simul., 2014, 40, 101-105.
[26] A. Gil-Villegas, A. Galindo, P.J. Whitehead, S.J. Mills, G. Jackson, Statistical associating fluid theory for chain molecules with attractive potentials of variable range, J. Chem. Phys. 106 (1997) 4168.
[27] P. Morgado, R. Bonifácio, L.F.G. Martins, E.J.M. Filipe, Probing the structure of liquids with ^{129}Xe NMR spectroscopy: *n*-alkanes, cycloalkanes, and branched alkanes, J. Phys. Chem. B 117 (30) (2013) 9014–9024.
[28] P. Morgado, L.F.G. Martins, E.J.M. Filipe, From nano-emulsions to phase separation: Evidence of nanosegregation in (Alkane + Perfluoroalkane) mixtures using 129Xe NMR Spectroscopy, PCCP 21 (2019) 3742–3751.
[29] P. Morgado, J. Barras, E.J.M. Filipe, From nano-seggregation to mesophases: probing the liquid structure of Perfluoroalkylalkanes with ^{129}Xe NMR Spectroscopy, PCCP 22 (2020) 14736–14747.
[30] P. Morgado, K. Shimizu, J.M.S.S. Esperança, P.M. Reis, L.P.N. Rebelo, J.N. Canongia Lopes, E.J.M. Filipe, Using ^{129}Xe NMR to probe the structure of ionic liquids, J. Phys. Chem. Letters 4 (2013) 2758–2762.
[31] J.C.G. Calado, E.J.M. Filipe, J.N.A.C. Lopes, J.M.R. Lúcio, J.F. Martins, L.F.G. Martins, Liquid mixtures involving cyclic molecules: Xenon + cyclopropane, J. Phys. Chem. B 101 (36) (1997) 7135–7138.
[32] E.J.M. Filipe, L.M.B. Dias, L.A.M. Pereira, J.C.G. Calado, R.P. Sear, G. Jackson, Shape effects in molecular liquids: phase equilibria of binary mixtures involving cyclic molecules, J. Phys. Chem. 101 (1997) 11243–11248.
[33] R.P.M.F. Bonifácio, E.J.M. Filipe, M.C. dos Ramos, F.J. Blas, L.F.G. Martins, On the behaviour of solutions of xenon in liquid cycloalkanes: solubility of xenon in cyclopentane, Fluid Phase Equilib. 303 (2011) 193–200.
[34] P. Tancréde, P. Bothorel, P.D. St. Romain, D. Patterson. Interactions in alkane systems by depolarized Rayleigh scattering and calorimetry. Part 1. Orientational order and condensation effects in n-hexadecane + hexane and nonane isomers. J. Chem. Soc., Faraday Trans. II 73 (1977) 15–28.
[35] M.B. Ewing, K.N. Marsh, Thermodynamics of mixtures of 2,3-dimethylbutane + cycloalkanes: a comparison with theory, J. Chem. Thermodyn. 9 (1977) 357–370.
[36] P.D. St. Romain, H.T. Van, D. Patterson, Effects of molecular flexibility and shape on the excess enthalpies and heat capacities of alkane systems, J. Chem. Soc., Faraday Trans. I 75 (1979) 1700-1707.
[37] B. Widom, Some topics in the theory of fluids, J. Chem. Phys. 39 (1963) 2808–2812.
[38] http://towhee.sourceforge.net
[39] D. Van Der Spoel, E. Lindahl, B. Hess, G. Groenhof, A.E. Mark, H.J.C. Berendsen, GROMACS: Fast, Flexible and Free., J. Comput. Chem. 26 (2005) 1701–1718.
[40] S. Pronk, S. Páll, R. Schulz, P. Larsson, P. Bjelkmar, R. Apostolov, M.R. Shirts, J.C. Smith, P.M. Kasson, D. van der Spoel, B. Hess, E. Lindahl, GROMACS 4.5: a High-Throughput and Highly Parallel Open Source Molecular Simulation Toolkit, Bioinformatics 29 (7) (2013) 845–854.
[41] M.G. Martin, J.I. Siepmann, Transferable potentials for phase equilibria. 1 United-atom description of *n*-alkanes, J. Phys. Chem. B 102 (1998) 2569.
[42] C.E.C. Laginhas, A.J. Palace Carvalho, J.P. Prates Ramalho, L.F.G. Martins, in: Proceedings of the 10th International Chemical and Biological Engineering Conference - CHEMPOR 2008 Braga, Portugal, September 4-6, 2008.
[43] M. Bohn, S. Lago, J. Fischer, F. Kohler, Excess properties of liquid mixtures from perturbation theory: results for model systems and predictions for real systems, Fluid Phase Equilib. 23 (1985) 137–151.
[44] I. Cibulka, T. Tkagi, *P-ρ-T* data of liquids: summarization and evaluation. 6. Nonaromatic hydrocarbons (C_n, $n \geq 5$) except *n*-alkanes C_5 to C_{16}, J. Chem. Eng. Data 44 (1999) 1105–1128.
[45] B. Hess, H. Bekker, H.J.C. Berendsen, G.E.M. Johannes, J.G.E.M. Fraaije, LINCS: a linear constraint solver for molecular simulations, J. Comput. Chem. 18 (1997) 1463–1472.
[46] E.C.W. Clarke, D.N. Glew, Evaluation of thermodynamic functions from equilibrium constants, Trans. Faraday Soc. 62 (1966) 539–545.